

Design and noise analysis of a sigma–delta capacitive micromachined accelerometer*

Liu Yuntao(刘云涛)^{1,2,†}, Liu Xiaowei(刘晓为)¹, Chen Weiping(陈伟平)¹, and Wu Qun(吴群)¹

(1 MEMS Center, Harbin Institute of Technology, Harbin 150001, China)

(2 College of Information and Communication Engineering, Harbin Engineering University, Harbin 150001, China)

Abstract: A single-loop fourth-order sigma–delta ($\Sigma\Delta$) interface circuit for a closed-loop micromachined accelerometer is presented. Two additional electronic integrators are cascaded with the micromachined sensing element to form a fourth-order loop filter. The three main noise sources affecting the overall system resolution of a $\Sigma\Delta$ accelerometer, mechanical noise, electronic noise and quantization noise, are analyzed in detail. Accurate mathematical formulas for electronic and quantization noise are established. The ASIC is fabricated in a $0.5\ \mu\text{m}$ two-metal two-poly n-well CMOS process. The test results indicate that the mechanical noise and electronic noise are $1\ \mu\text{g}/\sqrt{\text{Hz}}$ and $8\ \mu\text{V}/\sqrt{\text{Hz}}$ respectively, and the theoretical models of electronic and quantization noise agree well with the test and simulation results.

Key words: noise analysis; sigma–delta; micromachined; accelerometer; ASIC

DOI: 10.1088/1674-4926/31/5/055006

PACC: 0630G; 0710C

1. Introduction

High-resolution and high-precision accelerometers have a wide range of applications including earthquake detection, inertial navigation and guidance, microgravity measurements in space, GPS-augmented inertial navigation, biomedical applications and oil exploration^[1,2]. With the development of microelectromechanical systems (MEMS), closed-loop capacitive MEMS accelerometers have become very attractive due to their high sensitivity, low temperature sensitivity, low power consumption and wide dynamic range of operation^[3].

A sigma–delta ($\Sigma\Delta$) modulator is a particularly attractive way to implement a force feedback loop. $\Sigma\Delta$ modulators are very popular for low frequency applications where the over-sampling ratio can be considerably high and the noise rejection is very efficient. In micromachined accelerometers, the mechanical bandwidth is usually quite small ($< 2\ \text{kHz}$), and the $\Sigma\Delta$ conversion technique has become a very popular way to reduce noise and improve the performance of the sensor system. Besides, it provides a digital output and can be easily implemented in high-density CMOS technologies, and its one-bit feedback can solve the problem of nonlinear electrostatic forces^[4].

The extremely small signal at the output of the mechanical sensing element is a major challenge in MEMS accelerometer design, especially in the presence of large parasitics at the electromechanical interface. So the noise performance of the system is a primary concern in high-precision accelerometer design. In previous works, Lemkin^[5] analyzed the mechanical and electrical noise of a second-order $\Sigma\Delta$ accelerometer, but the work is just limited to the operational amplifier (op amp) and the first stage of the preamp noise. Kulah^[4] analyzed the different components of the electronic noise in detail, and pointed out that amplifier thermal noise and mass-residual

motion were the dominant factors in open-loop and closed-loop modes of operation respectively. However, in this work, all noise sources are treated individually, without considering their interaction. Recently, the effort has been focused on high-order electromechanical $\Sigma\Delta$, but the quantization noise in an electromechanical $\Sigma\Delta$ modulator is treated like that in a pure electronic $\Sigma\Delta$ modulator^[6,7]. In fact, due to the very low dc gain at low frequencies of the mechanical integrator, the noise shaping ability of the sensing element is very limited. So the quantization noise models in previous documents are very inaccurate. A detailed analysis and accurate models for the three noise sources are completed in this work.

2. Quasi-linear model of $\Sigma\Delta$ accelerometer and circuit design

A micromachined $\Sigma\Delta$ accelerometer is different from a pure electronic $\Sigma\Delta$ modulator, and it consists of a mechanical sensing element which has a continuous-time two-order low-pass characteristic, and a signal processing circuit which is a sampled-data system with discrete-time response. To establish mathematical models and formulas for the noise, a precise mathematical model for the overall system is required.

The system model developed in this work is shown in Fig. 1, where $G(z)$ is the mechanical transfer function of the sensing element in the discrete-time z -domain, and it can be expressed as^[6]

$$G(z) = K_f \frac{(1 - a_f z^{-1})z^{-1}}{(1 - b_f z^{-1})(1 - c_f z^{-1})}, \quad (1)$$

where K_f , a_f , b_f and c_f are gain, zero, and poles of the sensing element. Since K_f is very low, the sensing element has a weak quantization noise shaping ability compared with a second-order electronic integrator. The constant movement

* Project supported by the National High Technology Research and Development Program of China (No.2008AA042201).

† Corresponding author. Email: summer924@sina.com

Received 29 October 2009, revised manuscript received 23 December 2009

© 2010 Chinese Institute of Electronics

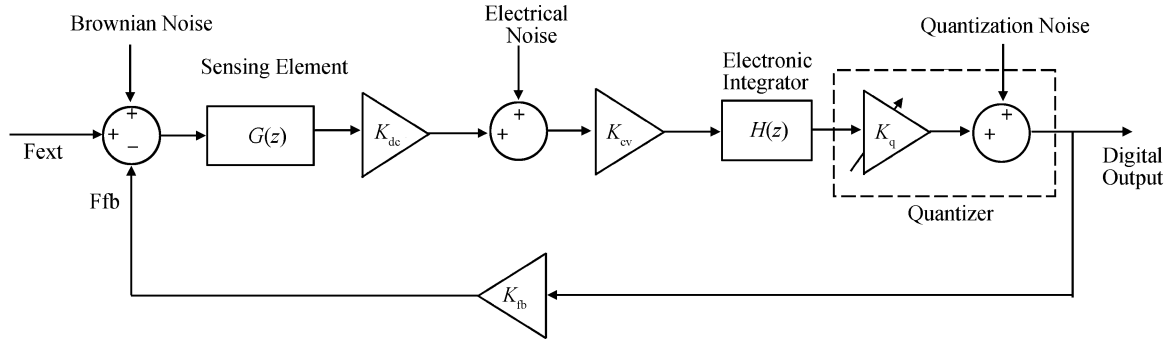


Fig. 1. Quasi-linear model of the $\Sigma\Delta$ accelerometer.

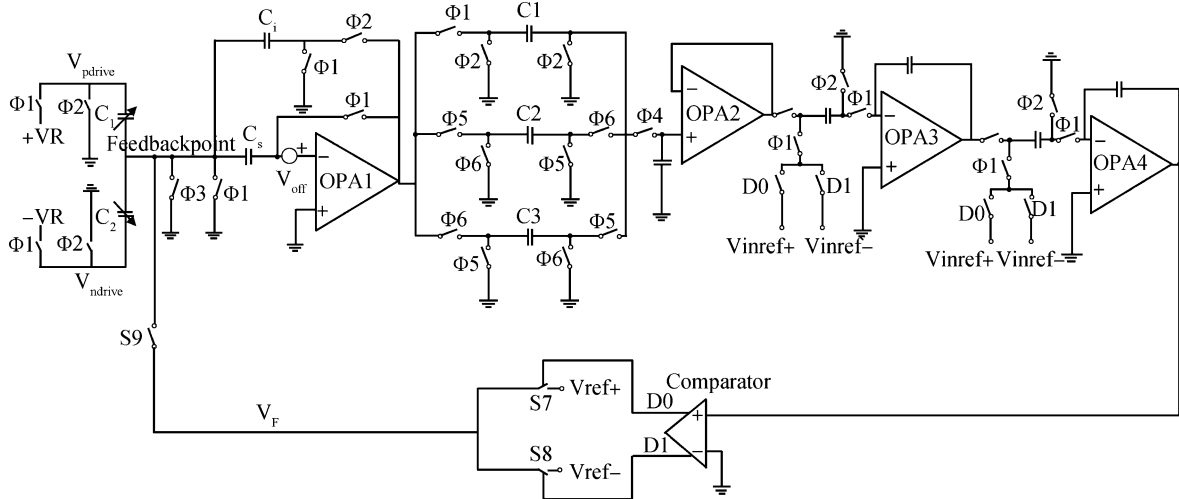


Fig. 2. Schematic diagram of the fourth-order $\Sigma\Delta$ interface circuit for the micromachined accelerometer.

of air molecules in the sensing element introduces Brownian noise to the system. K_{dc} is the gain of the displacement to variation of capacitance, and K_{CV} denotes the gain of the $C-V$ converter circuit that converts the change of capacitance to a voltage. The front-end circuit introduces electronic noise to the system. $H(z)$ expresses the electronic integrators which lead to a better quantization noise shaping. The single-bit quantizer with highly nonlinear behavior is modeled by a white noise source N_Q and a variable gain K_q . K_{fb} is the gain of the voltage to electrostatic force conversion on the proof mass in the feedback path.

Referring to Fig. 1, the transfer functions of the mechanical noise, electronic noise and quantization noise are respectively given by

$$MNTF(z) = \frac{K_{dc}K_{CV}H(z)K_qG(z)}{1 + K_{dc}K_{CV}H(z)K_qG(z)K_{fb}}, \quad (2)$$

$$ENTF(z) = \frac{K_{dc}K_{CV}H(z)K_q}{1 + K_{dc}K_{CV}H(z)K_qG(z)K_{fb}}, \quad (3)$$

$$QNTF(z) = \frac{1}{1 + K_{dc}K_{CV}H(z)K_qG(z)K_{fb}}. \quad (4)$$

According to Eqs. (2)–(4), the quantization noise is shaped by the sensing element and electronic integrators; the electronic noise is also shaped by the sensing element. However, the mechanical noise will not be shaped by the $\Sigma\Delta$ modulator, and goes directly to the output of the system.

The interface circuit is composed of a $C-V$ converter, a lead compensator, electronic integrators, a quantizer and a one bit D/A converter. A schematic diagram of the $\Sigma\Delta$ interface circuit is shown in Fig. 2. The switched-capacitor (SC) charge integration method is used for the $C-V$ converter based on the same foundation on which the SC circuit operates, and the sensed signal is insensitive to parasitic capacitance and undesirable charging^[8]. In order to compensate the finite gain of the op amp, reduce the $1/f$ noise and the offset of the op amp, a correlated double sampling (CDS) technique is introduced. However, CDS will induce broadband noise folding which is proportional to the bandwidth of op amp OPA1. Therefore, OPA1 must have low noise, moderate bandwidth and high slew rate. A low noise op amp designed in this work is shown in Fig. 3. A designed high-speed dynamic comparator is shown in Fig. 4, which utilizes a pre-amplifier with positive feedback and dynamic latch-up to realize a comparison function. The repetitive cycle of the clock includes four phases: charge-discharging phase, sensing phase, sampling phase and feedback phase. By the arrangement of the clock, the system can realize a closed-loop function without a feedback electrode.

3. Noise analysis

There are three main noise sources affecting the overall system resolution of a $\Sigma\Delta$ accelerometer: mechanical noise due to the Brownian motion of the proof mass, input-referred elec-

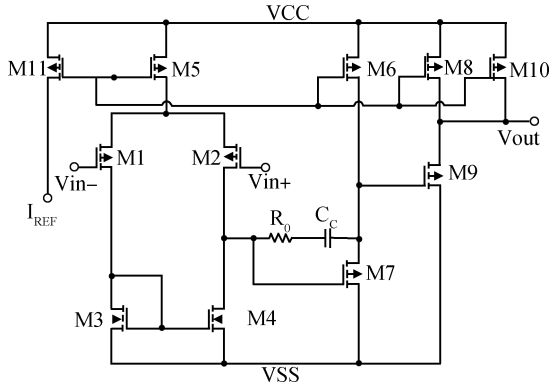


Fig. 3. Low noise operational amplifier.

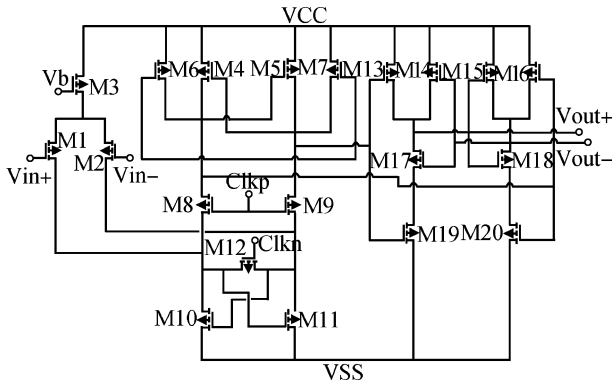


Fig. 4. High speed dynamic comparator.

tronic noise of the front-end interface and quantization noise from the analog to digital conversion process.

3.1. Mechanical noise

Mechanical noise is generated by the proof-mass itself, and it leads to an equivalent acceleration noise which can be expressed as^[5]

$$a_n = \frac{\sqrt{4kTb}}{m}, \quad (5)$$

where k is Boltzmann's constant, T the temperature in Kelvin, b the damping coefficient and m the proof-mass. As shown in Eq. (5), the mechanical noise depends on the parameters of the sensing element. Decreasing m and increasing k, b will reduce this noise considerably, so bulk silicon technology and vacuum packaging are effective ways.

3.2. Electronic noise

Electronic noise is generated by the front-end switched-capacitance (SC) charge integrator. Since CDS is employed in the SC circuit, the flicker noise ($1/f$ noise) and offset of the op amp are reduced considerably, and hence thermal noise is the dominant source. Also, CMOS transmission gates (TGs) are used to implement the switches to suppress charge injection and clock feed-through, but non-zero resistances of the CMOS switches generate wide-band thermal noise^[9].

Figure 5 shows the noise model of the charge integrator in the amplification phase. V_{st} is the thermal noise of resistance of the CMOS switch, V_n the input-referred noise of the op amp, R_s

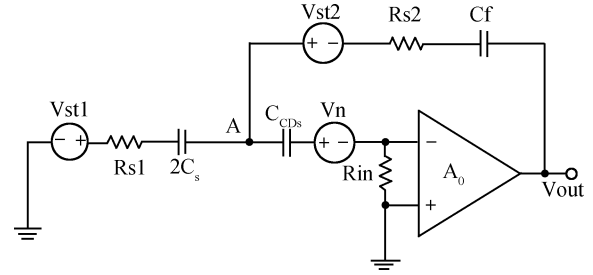


Fig. 5. Noise model of the charge integrator in the amplification phase.

the resistance of the switch, R_{in} the input resistance of the op amp, C_s the sensing capacitance, C_f the feedback capacitance and A_0 the DC gain of the op amp.

At the node A,

$$\frac{V_A - V_{st1}}{R_{s1} + \frac{1}{2sC_s}} + \frac{V_A - V_{out} - V_{st2}}{R_{s2} + \frac{1}{sC_f}} + \frac{V_A - V_n}{R_{in} + \frac{1}{sC_{CDS}}} = 0, \quad (6)$$

$$V_A = V_n - \frac{1 + sC_{CDS}R_{in}}{A_0 R_{in}sC_{CDS}} V_{out}. \quad (7)$$

Therefore,

$$V_{out} \left[\frac{2sC_s(1 + sC_{CDS}R_{in})}{(1 + 2sC_sR_{s1})A_0 R_{in}sC_{CDS}} + \frac{sC_f(1 + sC_{CDS}R_{in})}{(1 + sC_fR_{s2})A_0 R_{in}sC_{CDS}} + \frac{1}{A_0 R_{in}} + \frac{sC_f}{1 + sC_fR_{s2}} \right] = \left[\frac{2sC_s}{1 + 2sC_sR_{s1}} + \frac{sC_f}{1 + sC_fR_{s2}} \right] V_n - \frac{2sC_sV_{st1}}{1 + 2sC_sR_{s1}} - \frac{sC_fV_{st2}}{1 + sC_fR_{s2}}. \quad (8)$$

Since the DC gain and input resistance of the op amp are very large, $V_{out}(s)$ can be simplified to be

$$V_{out}(s) = \left[\frac{2C_s(1 + sC_fR_{s2})}{C_f(1 + 2sC_sR_{s1})} + 1 \right] V_n - \frac{2C_s(1 + sC_fR_{s2})V_{st1}}{C_f(1 + 2sC_sR_{s1})} - V_{st2}. \quad (9)$$

The amplification coefficient of charge integrator A is

$$A = -\frac{2C_s(1 + sC_fR_{s2})}{C_f(1 + 2sC_sR_{s1})}. \quad (10)$$

So, the input-referred noise of the front-end circuit is

$$V_{ni}(s) = -\left[1 + \frac{C_f(1 + 2sC_sR_{s1})}{2C_s(1 + sC_fR_{s2})} \right] V_n + V_{st1} + \frac{C_f(1 + 2sC_sR_{s1})}{2C_s(1 + sC_fR_{s2})} V_{st2}. \quad (11)$$

The power spectrum density (PSD) of the input-referred noise is given by

$$\frac{\overline{V_{ni}^2}(f)}{\Delta f} = \left[1 + \left(\frac{C_f}{2C_s} \right)^2 \frac{1 + (4\pi f C_s R_{s1})^2}{1 + (2\pi f C_f R_{s2})^2} \right]$$

$$+ \frac{C_f}{C_s} \frac{1 + 8\pi^2 f^2 C_s R_{s1} C_f R_{s2}}{1 + (2\pi f C_f R_{s2})^2} \left] \frac{\bar{V}_n^2(f)}{\Delta f} + \frac{\bar{V}_{st1}^2(f)}{\Delta f} + \left(\frac{C_f}{2C_s} \right)^2 \frac{1 + (4\pi f C_s R_{s1})^2}{1 + (2\pi f C_f R_{s2})^2} \frac{\bar{V}_{st2}^2(f)}{\Delta f}. \quad (12)$$

The input-referred thermal noise of the op amp shown in Fig. 3 can be expressed as

$$\bar{V}_n^2(f) = 2e_{nl}^2 \left[1 + \left(\frac{g_{m3}}{g_{m1}} \right)^2 e_{n3}^2 \right] \Delta f \approx 2e_{nl}^2 = \frac{16kT}{3g_{m1}} \Delta f, \quad (13)$$

and the thermal noise of resistance of the CMOS switch is

$$\bar{V}_{st}^2(f) = 4kTR_s \Delta f. \quad (14)$$

By replacing Eqs. (13), (14) in Eq. (12), the thermal noise PSD can be obtained as

$$\frac{\bar{V}_{ni}^2(f)}{\Delta f} = \left[1 + \left(\frac{C_f}{2C_s} \right)^2 \frac{1 + (4\pi f C_s R_{s1})^2}{1 + (2\pi f C_f R_{s2})^2} + \frac{C_f}{C_s} \frac{1 + 8\pi^2 f^2 C_s R_{s1} C_f R_{s2}}{1 + (2\pi f C_f R_{s2})^2} \right] \frac{16kT}{3g_{m1}} + 4kTR_{s1} + \left(\frac{C_f}{2C_s} \right)^2 \frac{1 + (4\pi f C_s R_{s1})^2}{1 + (2\pi f C_f R_{s2})^2} 4kTR_{s2}. \quad (15)$$

If $C_f = 2C_s$, $R_{s1} = R_{s2}$, and considering noise folding in the sampling process, the above equation can be simplified to be

$$\frac{\bar{V}_{ni}^2(f)}{\Delta f} = \left(\frac{64kT}{3g_{m1}} + 8kTR_s \right) \frac{2\pi f_u}{f_s}. \quad (16)$$

From Eqs. (15) and (16), it can be seen that the electronic noise mainly depends on the sampling frequency, and the ratio of C_f and C_s , increasing f_s and decreasing C_f/C_s can reduce the electronic noise, but it also increases the difficulty of design and may decrease the signal-to-noise ratio even though it decreases the absolute voltage noise.

3.3. Quantization noise

The electromechanical $\Sigma\Delta$ modulator should be designed in such a way that the quantization noise is much less significant than the other two noise sources^[10]. Based on Fig. 1 and considering the transfer function of the electronic integrator, QNTF(z) will be depicted as follows.

$$\text{QNTF}(z) = \left\{ 1 + K_{fb} K_{dc} K_{CV} G(z) \prod_{i=1}^{n-2} K_i [I(z)]^{n-2} K_q + \sum_{i=1}^{n-2} \prod_{j=i}^{n-2} K_i [I(z)]^{n-i-1} K_q \right\}^{-1}, \quad (17)$$

where n is the order of the electromechanical $\Sigma\Delta$ modulator, K_i the coefficients of the electronic integrators, $I(z) = z^{-1}/(1 - z^{-1})$ is the transfer function of an electronic integrator. For low frequencies ($f \ll f_s$), the QNTF(z) can be approximated by Eq. (18)^[11].

$$|\text{QNTF}(z)|_{f \ll f_s} \approx \left[|1 - z^{-1}|^n + |2 - b_f - c_f| |1 - z^{-1}|^{n-1} \right.$$

$$\left. + |(1 - c_f)(1 - b_f)| |1 - z^{-1}|^{n-2} \right] \times \left[K_{fb} K_{dc} K_{CV} K_f (1 - a_f) \prod_{i=1}^{n-2} K_i K_q + |(1 - c_f)(1 - b_f)| \prod_{i=2}^{n-2} K_i K_q \right]^{-1}. \quad (18)$$

Suppose that

$$\begin{cases} A = K_{fb} K_{dc} K_{CV} K_f (1 - a_f) \prod_{i=1}^{n-2} K_i K_q + |(1 - c_f)(1 - b_f)| \prod_{i=2}^{n-2} K_i K_q, \\ B = |2 - b_f - c_f|, \\ C = |(1 - c_f)(1 - b_f)|. \end{cases} \quad (19)$$

The quantization noise power in the signal bandwidth is

$$P_{QN} = \int_{-f_B}^{f_B} S_q^2(f) |\text{QNTF}(z)|^2 df = \int_{-f_B}^{f_B} \frac{2V_{fb}^2}{3f_s} |\text{QNTF}(z)|^2 df. \quad (20)$$

By replacing Eqs. (18), (19) in Eq. (20), the quantization noise power can be obtained as

$$P_{QN} = \frac{2V_{fb}^2}{3f_s} \frac{1}{A^2} \left[\frac{\pi^{2n}}{2n+1} \frac{1}{(\text{OSR})^{2n+1}} + (B^2 + 2C) \times \frac{\pi^{2n-2}}{2n-1} \frac{1}{(\text{OSR})^{2n-1}} + C^2 \frac{\pi^{2n-4}}{2n-3} \frac{1}{(\text{OSR})^{2n-3}} \right], \quad (21)$$

where $\text{OSR} = 2f_B/f_s$ is the over-sampling ratio, $2V_{fb}^2/3f_s$ is the power value of the unshaped quantization noise.

4. Results and discussion

In our design, the sensing element was fabricated by bulk silicon technology, and has the following parameters: mass $m = 1.2$ mg, damping coefficient $b = 0.0162$ kg/s, and spring stiffness $k = 120$ N/m. Test results indicate that its mechanical noise is about $1 \mu\text{g}/\sqrt{\text{Hz}}$.

According to the analysis above, a fourth-order $\Sigma\Delta$ interface circuit for a micromachined accelerometer was designed, as the sensing capacitance is 20 pF, to achieve optimal performance without increase in difficulty of design, the sampling frequency was chosen to be 150 kHz and the feedback capacitance 5 pF. The chip was fabricated in a 0.5 μm two-metal two-poly n-well CMOS process. Figure 6 shows a photograph of this chip.

To verify the electronic noise, the system works at open-loop mode and a fixed capacitance is attached to the interface circuit. Figure 7 is the spectrum of the output tested with an HP Hewlett Packard 35670A dynamic signal analyzer. The test result indicates that electronic noise is -102 dBV/ $\sqrt{\text{Hz}}$, equal to $8 \mu\text{V}/\sqrt{\text{Hz}}$. It is observed through the noise measurement that the CDS eliminates the $1/f$ noise significantly. According to Eq. (15), the theoretically predicted electronic noise is about $3 \mu\text{V}/\sqrt{\text{Hz}}$. It can be seen that the electronic noise model can

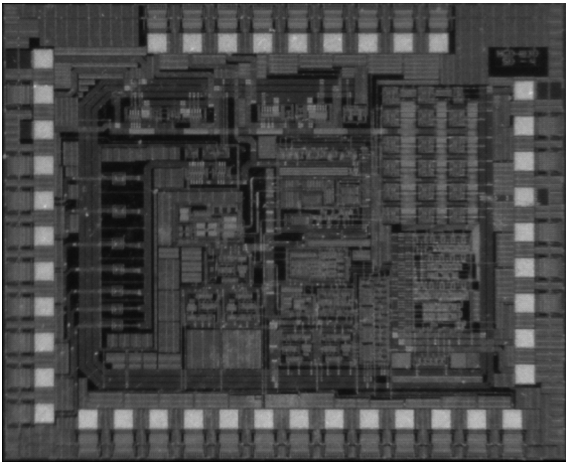


Fig. 6. Chip photograph of the fourth-order $\Sigma\Delta$ interface circuit (area: $4.6 \times 3.7 \text{ mm}^2$).

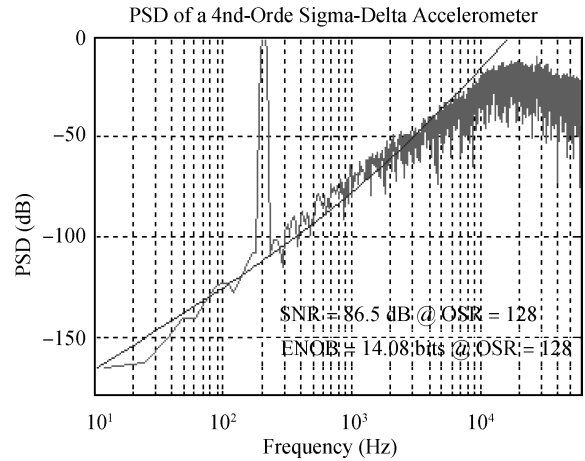


Fig. 9. Simulated and theoretically predicted PSD of quantization noise.

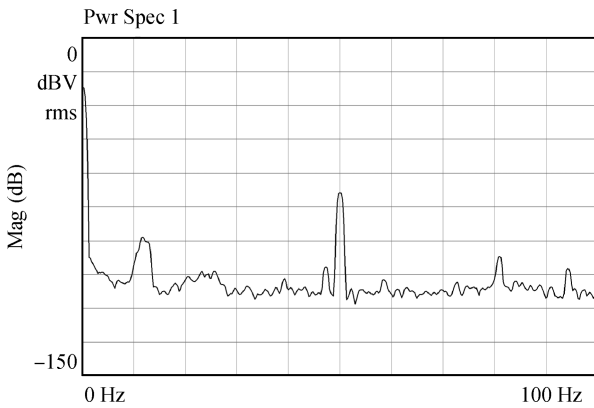


Fig. 7. Test results of electronic noise.

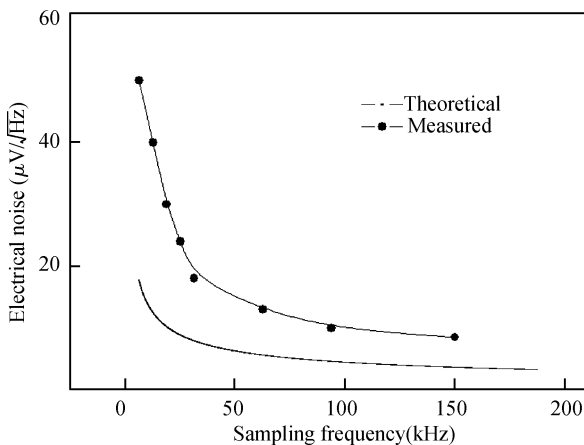


Fig. 8. Dependence of the electronic noise on sampling frequency .

predict this value well. Figure 8 shows the dependence of the electronic noise on sampling frequency. As shown in Fig. 8, although there is some difference between the measured and theoretical curves, the two curves have the same trend that with increasing sampling frequency the electronic noise decreases as expected in Eq. (15).

Since fourth-order $\Sigma\Delta$ modulator architecture is used, the

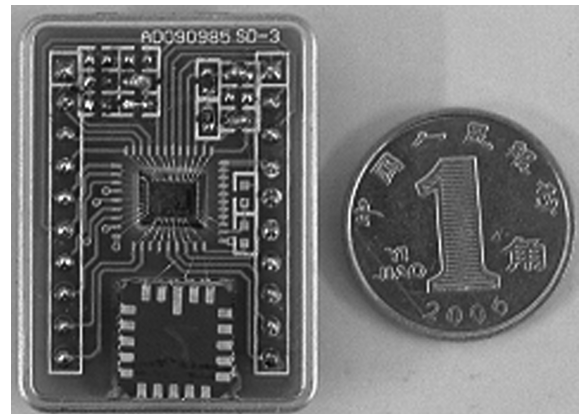


Fig. 10. Two chip integrated accelerometer.

Table 1. Summary of accelerometer characteristics.

CMOS interface ASIC	
Chip area	$4.6 \times 3.7 \text{ mm}^2$
Power consumption	40 mW
Sampling frequency	150 kHz
Offset of OP amp	0.6 mV
Resolution of comparator	1.5 mV
The MEMS accelerometer	
Sensitivity	1.2 V/g
Linear range	$\pm 2 \text{ g}$
Nonlinearity	0.2%
Open-loop noise floor	$12 \mu\text{g}/\sqrt{\text{Hz}}$
Closed-loop noise floor	$80 \mu\text{g}/\sqrt{\text{Hz}}$

quantization noise is attenuated considerably. To verify the quantization noise mathematical formula established in this work, a Matlab/Simulink model for the fourth-order $\Sigma\Delta$ accelerometer excluding mechanical and electronic noise was designed. Figure 9 shows the simulated and theoretically predicted power spectral densities of the output. As is obvious from Fig. 9, the simulation result approximates the theoretical model well.

The chip was combined with the bulk micromachined element on a printed circuit board (PCB), as shown in Fig. 10.

As the SC charge integrator is employed, the sensed signal is insensitive to parasitic capacitance. A summary of the accelerometer characteristics is shown in Table 1. It can be seen that the closed-loop noise floor is higher than the open-loop mode, which may be induced by residual motion of the proof-mass and the asymmetry between the two variable capacitances on the condition of no external force.

5. Conclusion

A fourth-order $\Sigma\Delta$ interface circuit for a micromachined accelerometer and a detailed analysis of the three main noise sources has been presented in this work. The test and simulation results agree well with the theoretical models. The mathematical formulas established in this work can provide a theoretical basis for the design of highly accurate $\Sigma\Delta$ micromachined accelerometers.

References

- [1] Lee W F, Chan P K. A capacitive-based accelerometer IC using injection-nulling switch technique. *IEEE Trans Circuits Syst*, 2008, 55(4): 980
- [2] Liu C H, Kenny T W. A high-precision wide-bandwidth micromachined tunneling accelerometer. *Microelectromechan Syst*, 2001, 10: 425
- [3] Kraft M, Lewis C, Hesketh T, et al. A novel micromachined accelerometer capacitive interface. *Sensors and Actuators A*, 1998, 68: 466
- [4] Kulah H, Chae J, Yazdi N, et al. Noise analysis and characterization of a sigma-delta capacitive microaccelerometer. *IEEE J Solid-State Circuits*, 2006, 41(2): 352
- [5] Lemkin M, Boser B E. A three axis micromachined accelerometer with a CMOS position-sense interface and digital offset-trim electronics. *IEEE J Solid-State Circuits*, 1999, 34: 456
- [6] Dong Y, Kraft M, Gollasch C, et al. A high-performance accelerometer with a fifth-order sigma-delta modulator. *Journal of Micromechanics and Microengineering*, 2005, 15: 22
- [7] Petkov V P, Boser B E. High-order electromechanical $\Sigma\Delta$ modulation in micromachined inertial sensors. *IEEE Trans Circuits Syst*, 2006, 53(2): 1016
- [8] Liu X W, Liu Y T, Chen W P, et al. A fourth-order sigma-delta interface circuit for closed-loop micromachined accelerometer. *Proceedings of the Eurosensors XXIII Conference*, 2009, 1: 1187
- [9] Oliaei O. Thermal noise analysis of multi-input SC-integrators for delta-sigma modulator design. *Proceeding of IEEE Int Symp Circuits and Systems*, 2000: 425
- [10] Lollar M, Michaeli L. Noise consideration for micromachined digital accelerometer. *Proceeding of IMTC*, 2006, 507
- [11] Dong Y, Kraft M, White W R. Higher order noise-shaping filters for high-performance micromachined accelerometers. *IEEE Trans Instrum Meas*, 2007, 56: 1666